AGU PUBLICATIONS

Radio Science

RESEARCH ARTICLE

10.1002/2014RS005466

Special Section:
Asia-Pacific Radio Science Conference - 2013

Ray tracing technique for global 3-D modeling of ionospheric electron density using GNSS measurements

Mohamad Mahdi Alizadeh[1], Harald Schuh[1,2], and Michael Schmidt[3]

[1]Institute of Geodesy and Geoinformation Science, Technische Universität Berlin, Berlin, Germany, [2]Department 1: "Geodesy and Remote Sensing", Helmholtz-Zentrum, Deutsches GeoForschungsZentrum, Potsdam, Germany, [3]Deutsches Geodätisches Forschungsinstitut, Technische Universität München, Munich, Germany

Key Points:
- Ionosphere modeling, Global Navigation Satellite Systems, ray tracing technique, and Formosat-3/Cosmic

Correspondence to:
M. M. Alizadeh,
mahdi.alizadeh@mail.tu-berlin.de

Citation:
Alizadeh, M. M., H. Schuh, and M. Schmidt (2015), Ray tracing technique for global 3-D modeling of ionospheric electron density using GNSS measurements, *Radio Sci.*, *50*, 539–553, doi:10.1002/2014RS005466.

Received 4 APR 2014
Accepted 28 APR 2015
Accepted article online 9 MAY 2015
Published online 28 JUN 2015

Abstract For space geodetic techniques, operating in microwave band, ionosphere is a dispersive medium; thus, signals traveling through this medium are in the first approximation, affected proportional to the inverse of the square of their frequencies. This effect allows gaining information about the parameters of the ionosphere in terms of total electron content (TEC) or the electron density (N_e). Making use of this phenomenon, space geodetic techniques have turned into a capable tool for studying the ionosphere in the last decades. Up to now, two-dimensional (2-D) models of Vertical TEC (VTEC) have been widely developed and used by different communities; however, due to the fact that these models provide information about the integral of the whole electron content along the vertical or slant raypath, these maps are not useful when information about the ionosphere at different altitude is required. This paper presents a recent study which aims at developing a global 3-D model of the electron density, using measurements from Global Navigation Satellite Systems and by applying the ray tracing technique to the upper atmosphere. The developed modeling approach represents the horizontal variations of the electron density, with two sets of spherical harmonic expansions of degree and order 15. The height dependency of the electron density is represented by a multilayered Chapman profile function for the bottomside and topside ionosphere, and an appropriate model for the plasmasphere. In addition to the geodetic applications of the developed models, within this study, the 3-D models of electron density can include geophysical parameters like maximum electron density and its corresponding height. High-resolution modeling of these parameters allows an improved geophysical interpretation, which is essential in all studies of the upper atmosphere, space weather, and for the solar-terrestrial environment.

1. Introduction

In the last decades, new technological systems, which transmit signals through the Earth's atmosphere, have been rapidly evolving that serve various purposes with relevance for our society, such as telecommunication, navigation, and surveillance systems. Among these systems, current space geodetic techniques, such as the Global Navigation Satellite Systems (GNSS), have found several applications in a broad range of commercial and scientific fields. The increase in using space geodetic techniques goes along with the demand for obtaining the most accurate and reliable results. This can be achieved by either technical improvements of the observing instruments or by minimizing the effect of the error sources. For this purpose, a special project called the Global Geodetic Observing System (GGOS) was established by the International Association of Geodesy in July 2003 (IAG, 2012, http://www.iag-ggos.org/).The main vision of GGOS is to integrate various space geodetic techniques, different models, and different approaches to ensure a long-term monitoring of geodetic, geophysical, and astronomical parameters. Following this global objective in geodetic science, this paper aims a global 3-D modeling of the upper atmosphere, the ionosphere, by using GNSS measurements.

To estimate the influence of the ionosphere, parameters of the ionosphere, i.e., total electron content (TEC) or the electron density (N_e), can be modeled. According to *Alizadeh et al.* [2011], some models are based on physical properties, e.g., the Global Assimilative Ionospheric Model [*Schunk et al.*, 2004]; others are empirical models, e.g., the International Reference Ionosphere (IRI) [*Bilitza and Reinisch*, 2007; *Bilitza et al.*, 2011] or NeQuick [*Hochegger et al.*, 2000; *Radicella and Leitinger*, 2001]; and finally, the mathematical models which are based on purely mathematical/statistical approaches. The corresponding model parameters could be calculated from space geodetic techniques and/or ionosonde data. Among these approaches are the TEC maps developed by the Analysis Centers (AC) of the International GNSS Service (IGS) (IGS, 2014, http://igscb.jpl.nasa.gov/).

Table 1. Examples of Base Functions/Mathematical Approaches for Multidimensional Modeling of the Ionosphere (λ: Longitude, φ: Latitude, h: Height, and t: Time)

Modeling	Parameter	Coverage	Base function	
2-D	VTEC(λ, φ)	global	Spherical Harmonics (SH)	
		regional	2-D B-splines	
3-D	VTEC(λ, φ, t)	global	2-D SH + Fourier function for time	
			trigonometric B-splines	
		regional	3-D B-splines	
	$N_e(\lambda, \varphi, h)$	global	2-D SH + function for height	empirical orthogonal function
				Chapman function
				Epstein function
4-D	$N_e(\lambda, \varphi, h, t)$	global	2-D SH + function for height + Fourier function for time	
		regional	4-D B-splines	

Therefrom, Global Ionosphere Maps (GIM) are developed as an official product of the IGS Ionosphere Working Group by performing a weighted mean of the various AC TEC maps [*Feltens*, 2003; *Hernández-Pajares et al.*, 2009]. Concentrating only on mathematical models, there are several ways to model the ionospheric parameters. Depending on the required parameter of the ionosphere, its dimension, and the area of the coverage, appropriate base functions should be chosen. Table 1 summarizes some of the mathematical approaches and base functions for different modeling techniques. Of course, the application of other procedures and base functions is also possible.

In this paper, we investigate global modeling of the electron density in 3-D, i.e., in longitude, latitude, and height. In the following, we first review the literature related to GNSS observations (section 2) and then introduce the modeling approach (section 3). Sections 4 and 5 describe different techniques for solving the unknown parameters and the estimation procedure. In section 6, sample results are presented; and in section 7, the results are assessed through different procedures. Finally, section 8 provides the conclusions and outlook of this paper.

Due to several developments and modifications of previous conceptual approaches proposed by, e.g., *Feltens* [1998] and due to the fact that this approach makes use of well-known, commonly accepted and widely used base functions that combine both mathematical and physical concepts, this study can be considered among the pioneers in applying ray tracing technique for global modeling of the upper atmosphere, using space geodetic techniques.

2. Literature Review

According to *Schaer* [1999], GNSS allows the determination of station specific ionosphere parameters in terms of slant TEC (STEC) values, using carrier phase, code, or the smoothed code measurements. To extract information about the ionosphere from GNSS observations, a linear combination is formed, which eliminates the geometric term. This linear combination is called geometry-free linear combination or the TEC observable. To form the ionospheric observable, simultaneous observations at two carrier frequencies L_1 and L_2 are subtracted. In this way along with the geometric term, all frequency-independent effects such as clock offsets and tropospheric delay are eliminated. This leads to an observable, which contains only the ionospheric refraction and the differential interfrequency hardware delays or the so-called differential code biases (DCBs). The geometry-free linear combination has the form

$$L_4 = k_{1,4}L_1 + k_{2,4}L_2 = L_1 - L_2 \,, \tag{1}$$

with $k_{1,4} = 1$ and $k_{2,4} = -1$.

Applying the above combination to the GNSS classical observation, equations [*Teunissen and Kleusberg*, 1998] lead to the geometry-free linear combination. Following *Schaer* [1999], this combination can also be applied to the smoothed code measurements, resulting in

$$\tilde{P_4} = \xi_4 I + c\left(\Delta b^S - \Delta b_R\right) \ , \tag{2}$$

where

$\xi_4 = 1 - f_{L1}^2/f_{L2}^2 \approx -0.647$ is a factor for converting the ionospheric refraction in L_4 to the refraction on L_1,
$\Delta b^S = b^{S,1} - b^{S,2}$ is the differential interfrequency hardware delay of the satellite S in time units, and
$\Delta b_R = b_{R,1} - b_{R,2}$ is the differential interfrequency hardware delay of the receiver R in time units.

For more details on code-carrier smoothing, refer to *Newby* [1992].

The ionospheric refraction I in equation (2) can be related to VTEC as a function of the geomagnetic latitude β and the Sun-fixed longitude s in the following way:

$$I = \xi_E \mathrm{STEC}(\beta, s) = \xi_E F(z) \mathrm{VTEC}(\beta, s) \ , \tag{3}$$

with

$F(z)$ is mapping function evaluated at zenith distance z,
$\xi_E = \frac{C_x}{2} f_1^{-2}$ ≈ 0.162 m/TECU (total electron content unit, 1 TECU $= 10^{16}$ el m^{-2}),

where $C_x = 80.6$ (m^3/s^2) [*Brunner and Gu*, 1991; *Datta-Barua et al.*, 2006]. By substituting equation (3) in equation (2), the ionospheric observable for code, phase, or the smoothed code measurements could be obtained

$$\tilde{P_4} \approx \xi_4 \xi_E F(z) \mathrm{VTEC}(\beta, s) + c\left(\Delta b^S - \Delta b_R\right) \ . \tag{4}$$

Equation (4) indicates the ionospheric observable for phase-smoothed code measurements. Note that the equation sign "=" in equation (4) has been replaced by the approximate equation sign "≈" because of including the simplified single-layer assumption, for more details refer to *Todorova* [2008].

3. Modeling Approach

In this study, we investigate modeling electron density in 3-D, i.e., in longitude, latitude, and height. To develop a 3-D global model for electron density, a spherical harmonic expansion up to degree and order 15 is used for longitude and latitude variations. For height dependency, several procedures can be applied.

To model the height variability of the electron density, one procedure is to apply empirical orthogonal functions (EOFs) introduced by *Fremouw et al.* [1992] and further improved by *Howe et al.* [1998]. *Rawer* [1988] as well as *Radicella and Leitinger* [2001] applied Epstein functions to represent the height dependencies. An alternative approach is applying a Chapman profile function to express the height variations of the electron density.

According to *Rishbeth and Garriott* [1969], the Chapman profile function describes the vertical structure of the electron density in the ionosphere under hydrostatic equilibrium assumption for the upper atmosphere. Applying the Chapman profile function, the electron density at each point can be computed from maximum electron density N_0 and its corresponding height h_0 along the raypath:

$$N_e(h, \chi) = N_0 \, e^{\alpha(1 - z - \sec \chi e^{-z})} \quad \text{and} \quad z = \frac{h - h_0}{H} \ , \tag{5}$$

where

$N_e(h, \chi)$ is the electron density at a desired point,
N_0 is the maximum electron density at $\chi = 0°$, i.e., the Sun at zenith,
h_0 is the reference height of maximum electron density at $\chi = 0°$,
H is the scale height,
χ is the Sun zenith angle, and
α is the recombination coefficient.

In equation (5), the Sun's zenith angle is taken into account; $\chi = 0°$ corresponds to local noon time. At local noon, the maximum electron density N_m achieves its maximum value N_0, equation (6), and the reference height h_m has its minimum value h_0. During the time of sunset and sunrise, h_m reaches its maximum and N_m its minimum. The relation between the electron density maximum N_m and its corresponding value at $\chi = 0°$, i.e., N_0 is derived by *Ratcliffe* [1972]

$$N_m = N_0(\cos\chi)^{\alpha}\ , \tag{6}$$

and the relation for h_m is given by

$$h_m = H\ln\{\sec\chi\} + h_0\ . \tag{7}$$

Replacing N_0 in equation (5) with the N_m from equation (6) leads to the specified form of Chapman profile function

$$N_e(h) = N_m\ \ e^{\alpha(1-z-e^{-z})} \qquad \text{and} \qquad z = \frac{h-h_m}{H}\ . \tag{8}$$

In equation (8), α is the recombination coefficient. *Chiu* [1975] proposed an empirical model that assumed a linear dependency between the loss rate and the electron density. This results α equal to unity. *Ezquer et al.* [1996] assumed two different behaviors for the bottomside and topside ionosphere. Similar to *Chiu* [1975], he assumed a linear relation between loss rate and electron density within the bottomside ionosphere. But in the topside, he presumed the loss rate proportional to the square of the electron density, resulting in $\alpha = 0.5$. Following this proposal, the used Chapman profile function will also be different for the bottomside and topside ionosphere. So for the bottomside ionosphere (i.e., for the E, F_1, and bottomside F_2 layer), we have $\alpha = 1$, and the Chapman function would be

$$N_e^{\text{bottom}}(h) = N_mF_2\ \ e^{\,(1-z-e^{-z})}\ . \tag{9}$$

This is known as the β Chapman function. For the topside ionosphere, the Chapman profile function would read

$$N_e^{\text{top}}(h) = N_mF_2\ \ e^{0.5(1-z-e^{-z})}. \tag{10}$$

This function is known as the α-Chapman function *Ratcliffe* [1972].

To represent electron density in plasmasphere, several models have been developed. Based on data from the NASA Radio Plasma Imager, *Huang et al.* [2004] developed a preliminary empirical model, which specified the electron density profile for a given location and time in the altitude range from ~ 2500 km to 5000 km. The model had a smooth transition at the interface from the topside ionosphere to the plasmasphere. *Jakowski et al.* [2002] proposed a model for topside ionosphere and plasmasphere (TIP) to improve the operational retrieval of vertical electron density profile from the CHAMP mission. The electron density $N_e(h)$ represented by TIP is described by

$$N_e(h) = N_mF_2\ \ e^{0.5(1-z-e^{-z})} + N_{P0}\ \ e^{(-h/H_P)}\ , \tag{11}$$

with

$$z = \frac{h-h_mF_2}{H_{\text{TS}}}\ , \tag{12}$$

where

h	is the height of a desired point,
N_mF_2, h_mF_2	are the ionosphere peak electron density and height,
H_{TS}	is the topside scale height, and
N_{P0}, H_P	are plasmasphere basis density and scale height.

In equation (11), the first term of the right-hand side covers the topside ionosphere/bottom of the plasmasphere and the second term for bottom of plasmasphere onward. Within our study, we apply a combination of the multilayer Chapman function and the TIP model to represent the electron density through the whole ionosphere:

$$N_e(h) = N_mF_2 \;\; e^{(1-z-e^{-z})} + N_mF_2 \;\; e^{0.5(1-z-e^{-z})} + N_{P0} \;\; e^{(-h/H_P)} \; . \tag{13}$$

In equation (13), the first term of the right-hand side is counted from bottomside ionosphere up to h_mF_2, the second term from h_mF_2 to top of the ionosphere/bottom of plasmasphere, and the third term from topside ionosphere/bottom of plasmasphere onward. Considering the smoothed code measurements from equation (2), according to the definition, STEC is the integral of electron density along the raypath from receiver R to satellite S

$$\mathrm{STEC} = \int_R^S N_e(s)\mathrm{d}s \; . \tag{14}$$

Inserting equation (14) into equation (4), the relation between TEC observable and the electron density yields

$$\tilde{P_4} = \xi \int_R^S N_e(h)\mathrm{d}s + c(\Delta b^S - \Delta b_R) + \varepsilon \; . \tag{15}$$

Note that $N_e(s)$ in equation (14) is approximated by $N_e(h)$ in equation (15), as we assume the variations of electron density to be explicitly depending on height. The variations in the horizontal component of electron density (i.e., in longitude and latitude) are implicitly indicated in the following section, where maximum electron density and height are represented by spherical harmonic base functions.

Substituting $N_e(h)$ from equation (13) into equation (15) yields

$$\tilde{P_4} = \xi \int_R^S \left(N_mF_2 \;\; e^{(1-z-e^{-z})} + N_mF_2 \;\; e^{0.5(1-z-e^{-z})} + \; N_{P0} \;\; e^{(-h/H_P)} \right) \mathrm{d}s + c(\Delta b^S - \Delta b_R) + \varepsilon \; . \tag{16}$$

Performing the integration over the defined layers would lead to

$$\begin{aligned} \tilde{P_4} = \xi \Bigg(& \int_R^{h_mF2} N_mF_2 \;\; e^{(1-z-e^{-z})}\mathrm{d}s + \int_{h_mF_2}^{h_{\text{Iono Top}}} N_mF_2 \;\; e^{0.5(1-z-e^{-z})}\mathrm{d}s \\ & + \int_{h_{\text{Iono Top}}}^{S} N_{P0} \;\; e^{(-h/H_P)}\mathrm{d}s \Bigg) + c(\Delta b^S - \Delta b_R) + \varepsilon \; . \end{aligned} \tag{17}$$

Equation (17) relates the smoothed GNSS TEC observable $\tilde{P_4}$ to the ionosphere/plasmasphere parameters along the raypath. In this equation, the parameters of the multilayer Chapman profile function, i.e., N_mF_2, h_mF_2, H_{TS}, N_{P0}, and H_P, as well as the receiver and satellite DCB (Δb_R and Δb^S), are the unknown parameters.

4. Solving the Unknown Parameters

Within this study, we concentrate only on the ionospheric parameters N_mF_2, h_mF_2, and H_{TS} by assuming the plasmaspheric parameters as known. Following *Jakowski et al.* [2002], the value for plasma scale height H_P is fixed at 10,000 km, and the plasmasphere basis density N_P is set equal to the electron density of the highest topside ionosphere, i.e., electron density at the height of 1000 km. Concerning the ionospheric scale height, following *Cappellari et al.* [1976], H_{TS} is assumed to be dependent only on h_mF_2 value and given by

$$H_{\mathrm{TS}} = \frac{5}{3}\left(30 + 0.2(h_mF_2 - 200)\right) \quad [km] \; , \tag{18}$$

where h_mF_2 is in kilometer. With these assumptions, our unknown parameters in equation (17) will be restricted to N_mF_2 and h_mF_2 parameters only.

To solve the unknown parameters of equation (17), *Feltens* [1998] performs the analytical integration along the raypath. In the first step, he assumes the ionosphere as a single-layer model and maps the integration

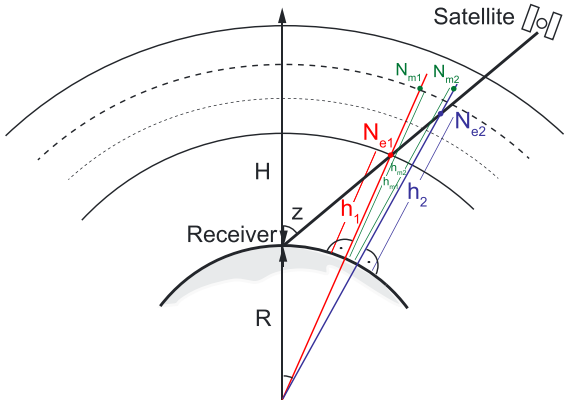

Figure 1. Concept of applying ray tracing technique to the Chapman profile function.

increment ds to vertical dh, introducing new integration increments by using the counter part to the Single Layer Model (SLM) mapping function $1/\cos(z)$, where z is the satellite zenith angle at the receiver point.

Following *Cappellari et al.* [1976], he then performs the analytical integration over the β-layer form of the Chapman profile function and obtains the relation between the TEC observable and the integral over the Chapman profile. In the next step, he takes the real form of ionosphere into account by assuming this medium as a spherical stratified layer. Therefore, he performs his calculations in different integration steps. This leads to a very sophisticated procedure, including several approximations, that in turn, makes the solution less accurate.

In this study, we investigated a new approach for solving the integral in equation (17). In this approach, ray tracing technique (see section 4.1) is applied to calculate the parameters of the integral along the raypath. Applying this technique, ionosphere is subdivided into several layers; and therefrom, the integral along the track, from the receiver R to the satellite S, turns into a simple summation along the step points of the raypath

$$\tilde{P_4} = \xi \left(\sum_{i=1}^{k} N_m F_{2i} \;\; e^{\alpha(1 - z_i - e^{-z_i})} \mathrm{d}s_i \Big|_{\text{bottomside}} + \sum_{i=1}^{l} N_m F_{2i} \;\; e^{\beta(1 - z_i - e^{-z_i})} \mathrm{d}s_i \Big|_{\text{topside}} \right) + c(\Delta b^S - \Delta b_R) + \varepsilon \;, \tag{19}$$

with

$$z_i = \frac{h_i - h_m F_{2i}}{H_i} \;, \tag{20}$$

where

$N_m F_{2i}$	is the maximum electron density at each step point,
$h_m F_{2i}$	is the height of maximum electron density at each step point,
H_i	is the scale height at each step point,
h_i	is the geocentric height of each step point, and
ds_i	is the differential increment of slant range at each step point.

In equation (19), the summation is performed in $k + l$ step points along the raypath, from the satellite to the receiver. Figure 1 depicts the concept of applying this technique.

4.1. Ray Tracing Technique

Ray tracing estimates the propagation of an electromagnetic wave through a medium. In contrary to the mapping function method, ray tracing estimates the delays for any arbitrary slant direction. In this technique, the propagation path of an electromagnetic wave in a 3-D Cartesian coordinate system is derived by the Eikonal equation [*Born and Wolf*, 1999]

$$\sum_{i=1}^{3} \left(\frac{\partial S}{\partial x_i} \right)^2 = n^2(x, y, z) \;, \tag{21}$$

where

S	is the signal path through the medium,
$x_i = \{x, y, z\}$	is the Cartesian coordinate, and
n	is the refractive index of the medium depending on (x,y,z).

The Eikonal equation is used to establish a ray tracing system to determine the raypath and the optical path. This equation can generally be written in Hamiltonian canonical formalism [*Nafisi et al.*, 2012].

Within our study, ray tracing technique is applied to the GNSS signals, propagating through the upper atmosphere. Assuming the geocentric Cartesian coordinates of the receiver and the satellites position as the known parameters, ray tracing is applied to each of the observations between IGS ground stations and the observed GNSS satellites at each observation epoch. The ray tracing equation systems are solved for every single raypath, and the parameters of the trajectory and their corresponding path length are calculated. Finally, the required parameters of the Chapman profile function (equation (19)) are calculated. These parameters include the geocentric coordinates of the intersection points of signal path and the stratified layers of the ionosphere, slope distance between the two successive intersection points ds_i, geocentric height of each intersection point h_i, and satellite zenith angle at each intersection point. Furthermore, the solar zenith angle χ at each intersection point is also calculated and can be used when applying the general form of Chapman function (equation (5)).

4.2. Simulating Input Data

Due to the fact that the real observations usually contain uncertainties and random errors, to avoid inconsistencies in the input data and to focus only on the model and the procedure for estimating the unknown parameters, we simulate the GNSS input data.

According to definition, STEC is related to VTEC by a mapping function

$$\mathrm{STEC} = F(z')\mathrm{VTEC}\ , \tag{22}$$

where z' is the satellite zenith angle at Ionospheric Pierce Point (IPP). Taking equations (4) and (19) into account and substituting STEC by VTEC from equation (22), we get the simulated observation equation in which the terms representing DCB can also be neglected; so the equation simplifies to

$$F(z')\mathrm{VTEC} = \sum_{i=1}^{k} N_m F_{2i}\ \ e^{\alpha(1 - z_i - e^{-z_i})}\mathrm{d}s_i\Big|_{\text{bottomside}} + \sum_{i=1}^{l} N_m F_{2i}\ \ e^{\beta(1 - z_i - e^{-z_i})}\mathrm{d}s_i\Big)\Big|_{\text{topside}}\ . \tag{23}$$

Equation (23) is our observation equation for further computations.

Within our study, the simulation of input data is accomplished in two different steps. In the first step, GNSS observations from all the selected IGS stations are downloaded from, e.g., Crustal Deformation Data Information System ftp site (CDDIS, 2011, ftp://cddis.gsfc.nasa.gov/) in RINEX format. Splitting the observations into 2-hourly time intervals, the GNSS satellite observed at each IGS station are determined, and their precise orbital coordinates are extracted from the IGS precise satellite orbits (SOPAC, 2011, ftp://garner.ucsd.edu/pub/rinex/).

The raypaths between receiver and satellite are calculated using the coordinates of the stations and the satellites above 5° elevation angle observed at each station. Figure 2 depicts the GNSS raypaths observed from approximately 160 IGS stations at day 182, 2010, from 0 to 2 UT. The total number of raypaths for this time span was approximately 5180.

In the second step of simulation, the step-point heights are selected according to equation (13), by assuming three different profile functions for bottomside ionosphere, topside ionosphere, and for the pl asmasphere.

$$h_{i+1} = h_i + \mathrm{d}h_i\ , \quad i = 1, 2, \ldots, k\ , \tag{24}$$

where

$$\mathrm{d}h_i = \begin{cases} 50\ \mathrm{km} & h_i < 250\ \mathrm{km} \\ 100\ \mathrm{km} & 250 \le h_i < 1000\ \mathrm{km} \\ 100\ \mathrm{km} & 1,000 \le h_i \le 2000\ \mathrm{km}. \end{cases} \tag{25}$$

The starting height at the ionosphere's bottomside is set to $h_i = 50$ km. The bottomside extends then up to $h_m F_2 = 250$ km, and the ionosphere's topside from $h_m F_2 = 250$ km to $h_i = 1000$ km. The effective

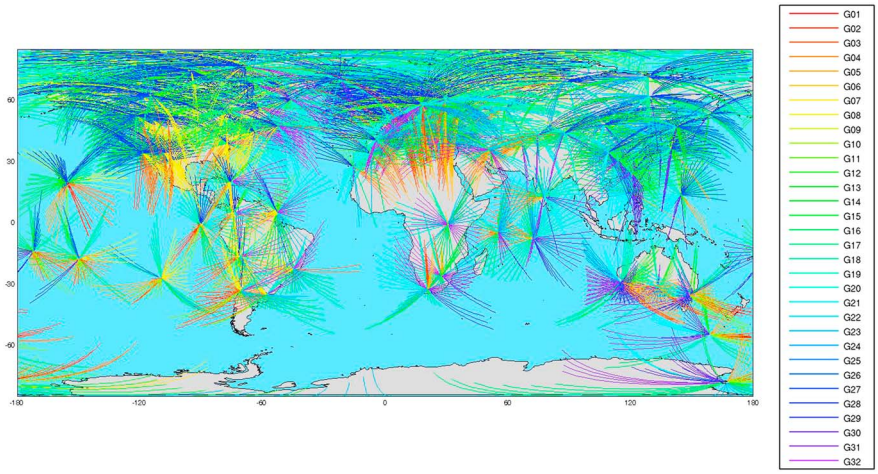

Figure 2. Input data with true GNSS raypaths but simulated values from IGS GIM at day 182, 2010 [0,2] UT (legend shows satellite Vehicle number of simulated GNSS satellites).

plasmaspheric part is assumed to reside within the height range from 1000 km to 2000 km; therefore, the model height range is limited to 2000 km.

After calculating the geocentric heights of the step points, the coordinates of each step point are calculated using ray tracing technique (see section 4.1). Therefore, the true positions of all step points and satellites at each epoch are consequently computed. In the next step, the coordinates of all IPP (with $h = 450$ km) are extracted from the step points of each raypath, and the VTEC values of these points are calculated from the IGS GIM, using the bivariate interpolation proposed by *Schaer et al.* [1998]. From long-term analysis, it is believed that the IGS VTEC maps have an accuracy of few TECU in areas well covered with GNSS receivers; conversely, in areas with poor coverage, the accuracy can be degraded by a factor of up to 5 [*Feltens et al.*, 2010]. Finally, STEC is derived by mapping VTEC to the slant path using equation (22). The computed STEC serves as the simulated observation for equation (23).

5. Estimation Procedure

5.1. Calculating A Priori Values

The observation equation (equation (23)) contains several parameters of which the a priori values should be known prior to the estimation procedure. These parameters include slope distance between the consecutive step points, ds_i, and the geocentric height of the step points, h_i, which are calculated using the ray tracing technique. The a priori values for the initial unknown parameters, i.e., N_mF_{2i} and h_mF_{2i} in equation (23) are calculated using the IRI 2012 model [*Bilitza et al.*, 2011; IRI, 2014, ftp://nssdcftp.gsfc.nasa.gov/models/]. Within this study, the software package for performing ray tracing calculations was developed by Dr. Dudy D. Wijaya based on fundamental equations described in *Wijaya* [2010]. The package is declared from the main function, and after carrying out the calculations, its results are appended to the station-wise information for further computations.

5.2. Global Representation of Unknown Parameters

According to equation (19) for each step point along the raypath, one individual N_mF_{2i} and h_mF_{2i} should be calculated. This is also shown schematically in Figure 1. Therefore, for each raypath, i.e., for each observation, we will have two sets of unknown parameters, which obtain k number of unknowns each. Thus, for each observation equation, we will have $2k$ unknown parameters. This in fact, turns our model into an underdetermined situation, and the problem becomes unsolvable.

However, these different N_mF_{2i} (or h_mF_{2i}) are not completely individual unknowns, but in principle, they are related to each other. The different N_mF_{2i} and h_mF_{2i} values could be represented by a set of base functions, i.e., one base function for N_mF_{2i}, and one for h_mF_{2i}. In this study, as we aim to model electron density globally, we use spherical harmonic base functions for representing the unknown parameters as

$$N_mF_{2i} = \sum_{n=0}^{n_{max}} \sum_{m=0}^{n} \tilde{P}_{nm}(\sin\beta_i)\left(a_{nm}\cos(ms_i) + b_{nm}\sin(ms_i)\right) \quad , \tag{26}$$

$$h_m F_{2i} = \sum_{n=0}^{n_{\max}} \sum_{m=0}^{n} \tilde{P}_{nm}(\sin \beta_i) \left(a'_{nm} \cos(ms_i) + b'_{nm} \sin(ms_i) \right) , \quad (27)$$

where

a_{nm}, b_{nm} are unknown coefficients of first spherical harmonics expansion,
a'_{nm}, b'_{nm} are unknown coefficients of second spherical harmonics expansion,
β_i is the geomagnetic latitude of each step point,
s_i is the Sun-fixed longitude of each step point, and
$\tilde{P}_{nm}$ is the normalized Legendre function of degree n and order m.

Applying these representations, the unknown parameters would reduce from $2k$ to the number $2(n_{\max} + 1)^2$ of spherical harmonic coefficients, and the model gets solvable.

5.3. Least Squares Estimation of the Unknown Parameters

The least squares estimation of the unknown parameters, namely the coefficients of two sets of spherical harmonic expansions, is applied to the simulated input data equation (23). As we have two sets of unknown parameters, we accomplish the estimation procedure in two steps. In the first step, we assume $h_m F_2$ as a known parameter by using its a priori values from IRI-2012 model and estimate the spherical harmonic coefficients related to $N_m F_2$ only. As the observation equation (equation (23)) is linear with respect to $N_m F_2$, there is no need for iteration, and the coefficients are obtained after performing the least squares adjustment only once. The estimated coefficients are then used to calculate the estimated $\hat{N}_m F_2$ values, which will be assumed as a known parameter for the next step.

In the next step, the coefficients related to $h_m F_2$ are estimated. For this, the a priori N_m values from IRI are replaced by their estimated $\hat{N}_m F_2$ values from the previous step. The estimation is accomplished in an iterative procedure, as the observation equation (equation (23)) is nonlinear with respect to h_m. In this study, the estimation procedure was accomplished in five iterations in order to achieve the empirical tolerance range of 2 TECU for the estimated residuals. After each iteration, the estimated coefficients are used for calculating the estimated $\hat{h}_m$ values. Within our study, we have not taken into account the correlation between the two unknown parameters, i.e., $N_m F_2$ and $h_m F_2$. This will be a matter of our further investigations.

5.4. Applying Constraints

In the estimation procedure, due to the fact that GNSS observations are relatively insensitive to height variations, some constraints should be applied to avoid obtaining unrealistic large residuals. As the unknown parameters $N_m F_2$ and $h_m F_2$ are presented by spherical harmonic expansion according to equation (26) and (27), we apply two sets of constraints, namely, global mean constraint and *sin*-surface function constraint.

As shown by *Schaer* [1999], the global mean value of a parameter expressed by spherical harmonic expansion is generally represented by the 0° spherical harmonic coefficient. So we can write

$$\bar{N}_m = a_{00} \quad \text{and} \quad \bar{h}_m = a'_{00} , \quad (28)$$

where $\bar{N}_m$ and $\bar{h}_m$ are the mean value of the global $N_m F_2$ and $h_m F_2$ distribution. a_{00} is the 0° spherical harmonic coefficient for representing $N_m F_2$, and a'_{00} is the 0° spherical harmonic coefficient for representing $h_m F_2$. Using the a priori values from the IRI model, the mean values of $N_m F_2$ and $h_m F_2$ in global distribution are calculated by

$$\bar{N}_m^{\mathrm{IRI}} = \sum \frac{N_m F_2^{\mathrm{IRI}}}{n} , \quad (29)$$

$$\bar{h}_m^{\mathrm{IRI}} = \sum \frac{h_m F_2^{\mathrm{IRI}}}{n} , \quad (30)$$

where

$N_m F_2^{\mathrm{IRI}}$, $h_m F_2^{\mathrm{IRI}}$ are the peak parameters from IRI model at the simulated points (see section 4.2), and
n is the number of global peak parameters.

Within this study, the global mean constraints are applied for estimating both $N_m F_2$ and $h_m F_2$ values.

In addition to the global mean constraint, a sin-surface function can be applied as a constraint to the observation equation system to bound the variations of the estimated parameters. The surface function forces

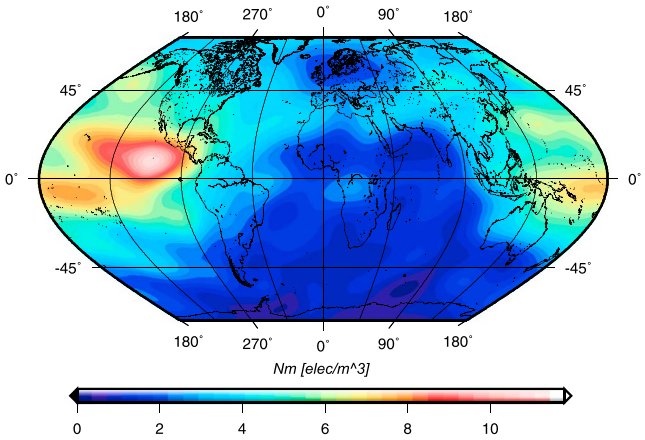

Figure 3. Estimated maximum electron density ($\times 10^{11}$elec/m^3) for day 182, 2010 [0,2] UT.

the estimated parameters to get values in a predefined range. Since the surface function affects nonlinear parameters, we apply this constraint for estimating h_mF_2 values only. According to *Feltens* [1998], h_0 can be expressed as

$$h_0 = \xi(x,y) = h_{0_{\min}} + \frac{h_{0_{\max}} - h_{0_{\min}}}{2}\left(1 + \sin(f(x,y))\right), \tag{31}$$

with

$h_0 = h_m - H.\ln\{\sec\chi\}$	is the height of maximum electron density at noon (i.e., $\chi = 0°$),
χ	is the solar zenith angle, and
$h_{0_{\max}}, h_{0_{\min}}$	are the predefined range for h_0 variations.

Feltens [1998] proposed $h_{0_{\min}} = 400$ km, and $h_{0_{max}} = 450$ km. Within this study, we assume a wider range by applying

$$\begin{aligned} h_{0_{\min}} &= 200 \text{ km} \\ h_{0_{\max}} &= 550 \text{ km}\ . \end{aligned} \tag{32}$$

The inner sin function in equation (31) is expressed by

$$f(x,y) = c\ \sin(x+y) + v_x \sin^2 x \cos x + \mu_x \sin x \cos^2 x + v_y \sin^2 y \cos y + \mu_y \sin y \cos^2 y\ , \tag{33}$$

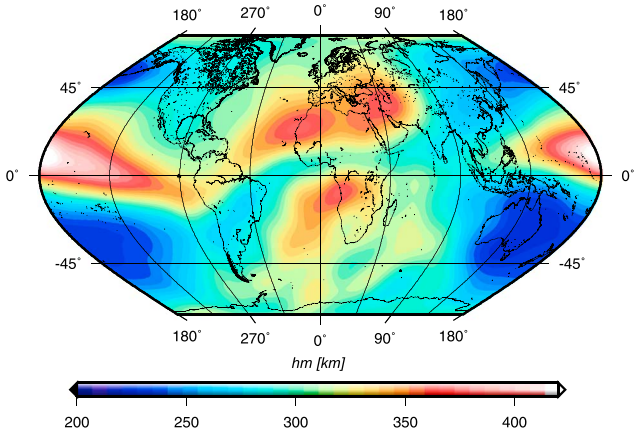

Figure 4. Estimated maximum electron density height (km) for day 182, 2010 [0,2] UT.

where

$c = 0.001$	is the small numerical constant,
$x = \varphi_m$	is the geomagnetic latitude, and
$y = \tau/2$	is the local time.

In equation (33), v_x, μ_x, v_y, and μ_y are four coefficients which should be solved prior to applying the constraint. For this, we select four random sample points globally and calculate their x, y, χ, and h_m values from the IRI model. Assigning equation (33) for each of these points, we obtain a linear equation system of four equations and four unknowns. By solving this linear equation system, the four unknown

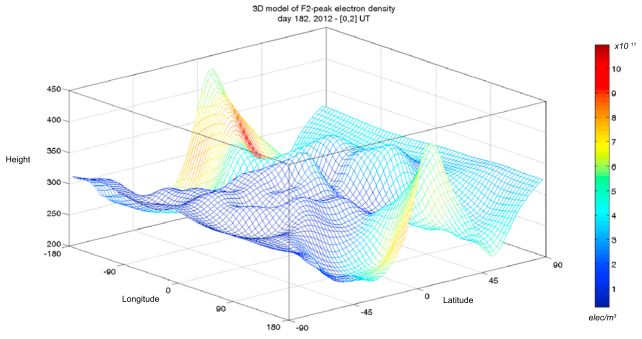

Figure 5. Three-dimensional model of F_2 peak electron density for day 182, 2010 [0,2] UT; color bar indicates the maximum electron density ($\times 10^{11}$ elec/m^3), and the Z axis indicates maximum electron density height in km.

coefficients of equation (33) are obtained. The sin function in equation (33) restricts the output values to a range of $[-1, 1]$, and the inner function $f(x, y)$, removes the effect of 2π period of *sin* function, which could make the convergence unstable.

To apply the constraints within the least squares estimation procedure, the design matrix (A) and the misclosure vector (w) are modified correspondingly.

6. Results

After estimating the unknown coefficients of two sets of spherical harmonic expansion, the final unknown parameters (i.e., $\hat{N}_m F_2$ and $\hat{h}_m F_2$) are calculated using equations (26) and (27). $\hat{N}_m F_2$ and $\hat{h}_m F_2$ are then depicted in a global grid-wise map with a spatial resolution of 2.5° in latitude and 5° in longitude, and temporal resolution of 2 h. To achieve this spatial resolution, the degree and order of spherical harmonic expansion is set to 15. This leads to estimation of 256 coefficients for every single 2-hourly map. Thus, the unknown parameters will be modeled in 12 two-hourly maps for a whole day. Nevertheless, depending on the available observations and the computation time, selecting less time span is also possible. So applying these conditions we have 2 times 256 or 512 unknown parameters for each 2 h map; and for the whole day, we will have 12 times 512 or 6144 unknown parameters. To solve these parameters, a MATLAB-based software was developed which provides the estimated parameters in 12 two-hourly maps for a complete day solution.

Figure 3 depicts the global grid-wise values of the estimated $\hat{N}_m F_2$ for the sample day 182 of 2010 at [0, 2] UT. Figure 4 shows the corresponding $\hat{h}_m F_2$ values.

The related $\hat{N}_m F_2$ and $\hat{h}_m F_2$ values shown in Figures 3 and 4 are depicted in a 3-D conjunction plot (Figure 5) to illustrate a better understanding of the estimated electron density parameters.

7. Assessment of Results

The estimated $\hat{N}_m F_2$ and $\hat{h}_m F_2$ are assessed through different procedures. First, the accuracy of the estimated values from least squares adjustment is evaluated using their standard deviation values. Then the estimated values are compared with the maximum electron density, and its corresponding height is derived from the IRI model. Finally, the estimated values are cross validated using the F_2 peak parameters derived from the Formosat-3/COSMIC (F/C) measurements.

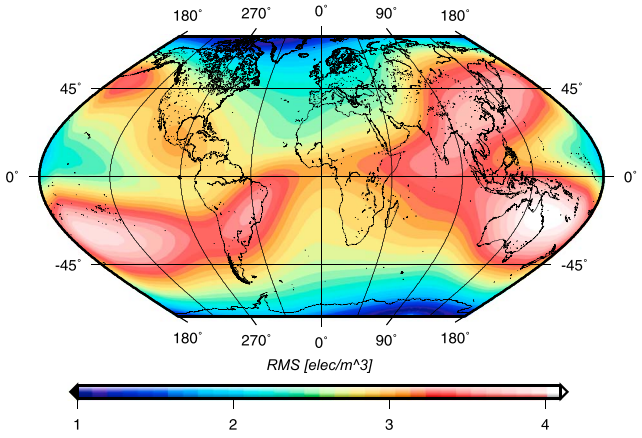

Figure 6. RMS map of estimated maximum electron density ($\times 10^{10}$ elec/m^3) for day 182, 2010 [0,2] UT.

7.1. Accuracy of Estimated Parameters

In the course of least squares estimation procedure, the accuracy of the estimated parameters is obtained from the covariance matrix of the estimated parameters. Since in our procedure we estimate the coefficients of the spherical harmonic expansions, equations (26) and (27), to obtain the accuracy of the estimated parameters, i.e., $\hat{N}_m F_2$ and $\hat{h}_m F_2$, we have to apply the variance-covariance propagation law to the spherical harmonic expansions. The calculated values which represent the standard deviation of the

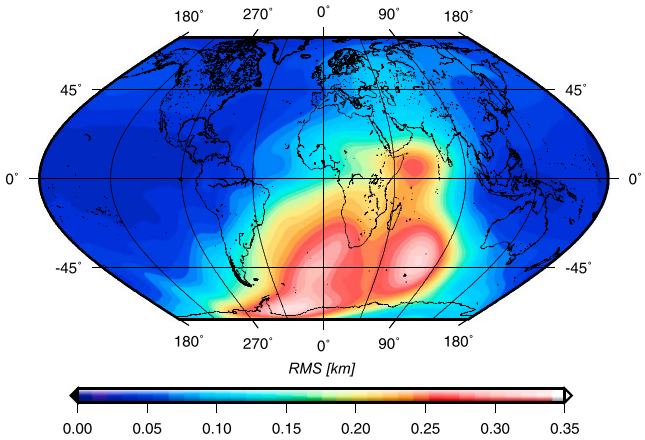

Figure 7. RMS map of estimated maximum electron density height (km) for day 182, 2010 [0,2] UT.

estimated parameters are illustrated as global grid-wise maps with the same spatial and temporal resolution as the estimated parameters themselves, i.e., spatial resolution of 2.5° in latitude and 5° in longitude, and temporal resolution of 2 h. These maps are usually known as the root-mean-square (RMS) maps. For more details, refer to *Alizadeh* [2013].

Figure 6 depicts the RMS map of $\hat{N}_m F_2$ for day 182 of 2010 at [0,2] UT. Figure 7 shows the RMS map of $\hat{h}_m F_2$ for the same day.

Taking Figure 6 into account, the standard deviation of estimated electron density $\hat{N}_m F_2$ at day 182, 2010, [0,2] UT, varies between 1.019×10^{10} elec/m^3 and 4.093×10^{10} elec/m^3 globally. The mean and standard deviation of the $\hat{N}_m F_2$ standard deviation is 2.587×10^{10} elec/m^3 and 7.080×10^9 elec/m^3, respectively. The highest-standard deviation values, corresponding to the lowest accuracy of the estimated $\hat{N}_m F_2$ can be seen at southern midlatitude region, at the outer skirts of the highest-maximum electron density values for this special time interval, i.e., between 0 and 2 UT (see Figure 3).

Considering the height of maximum electron density (Figure 7) the standard deviation of the estimated $\hat{h}_m F_2$ at the same time interval varies between 0.021 km and 0.327 km on the whole globe, with a mean value of 0.104 km. Taking Figure 7 into account, the highest-standard deviation values (corresponding to lowest estimation accuracy) are detected at the middle and high-southern latitudes. This can be attributed to the sparse data coverage in considerable parts on the Southern Hemisphere due to real GNSS tracks used in the simulation procedure.

7.2. Comparison With F/C Peak Parameters

In the previous section, the estimated $\hat{N}_m F_2$ and $\hat{h}_m F_2$ were compared to the $N_m F_2$ and $h_m F_2$ values derived from the IRI model. But as the IRI model is used to derive the a priori values of some of the input parameters, the estimated parameters are further compared to the electron density peak parameters derived from F/C occultation data.

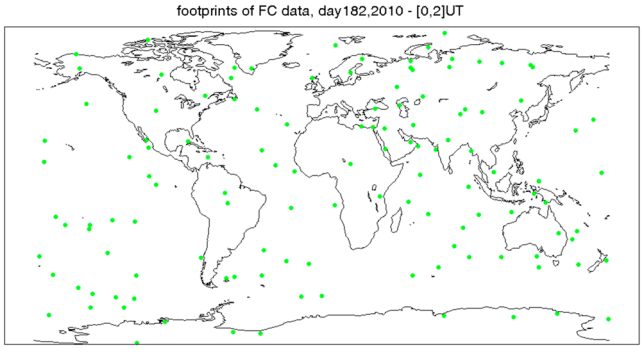

Figure 8. Footprints of F_2 peak parameters obtained from F/C data, for day 182, 2010 [0,2] UT.

For this study, the F/C F2-peak parameters were provided by Professor Lung-Chi Tsai from the Ionolab of Taiwan National University [*Tsai*, 2012]. The F/C peak parameters are provided in terms of F_2 peak height $h_m F_2$ and F_2 critical frequency $f_0 F_2$, obtained from the F/C radio occultation measurements. According to *Tsai et al.* [2011], to derive the F_2 peak parameters, the

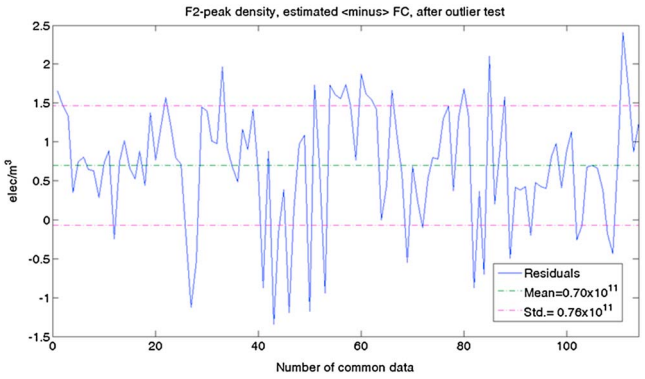

Figure 9. F_2 peak electron density deviations of estimated minus F/C, for day 182, 2010 [0,2] UT.

electron density profile is obtained individually for the ionosphere below the F/C orbital height and for the ionosphere above the F/C orbital height. The profile below the F/C height is computed directly from the measured occultation data. To obtain the topside profile, electron density is extrapolated above the height of the F/C, using an exponential extrapolation.

To compute the maximum electron density from the F/C data, a simple formula is applied to the measured f_0F_2 [*Davies*, 1990]

$$N_mF_2 = \frac{1}{80.6}(f_0F_2)^2 \ . \tag{34}$$

Figure 8 shows the footprints of F_2 peak parameters obtained from F/C radio occultation measurements. Performing the comparison at the common points, Figure 9 shows the deviations of estimated minus F/C data maximum electron density. Figure 10 depicts the corresponding deviations of maximum electron density height. The mean deviation of estimated maximum electron density minus F/C maximum electron density for day 182, 2010 [0,2] UT is 0.70×10^{11} elec/m^3 with a standard deviation of 0.76×10^{11} elec/m^3. The mean residual of estimated minus F/C of the maximum electron density height for the same day is $\sim$ 40.8 km with a standard deviation of 38.3 km.

To evaluate this difference, the test of significance is performed over the deviation values, i.e., deviations of the estimated peak parameters minus F/C derived peak parameters. Prior to performing this statistical test, an outlier test with a probability level of 10% is performed over the F/C raw data and the outliers are eliminated. The test of significance is then performed, over the two deviation values. The statistic z for each of the estimated parameter reads

$$z = \frac{\bar{x} - \mu}{s/\sqrt{n}} \ , \tag{35}$$

where

$\bar{x}$ is the mean value of the estimated minus F/C deviations,
μ is the expectation value of the estimated minus F/C deviations,
s is the standard deviation of the estimated minus F/C deviations, and
n is the number of common data points.

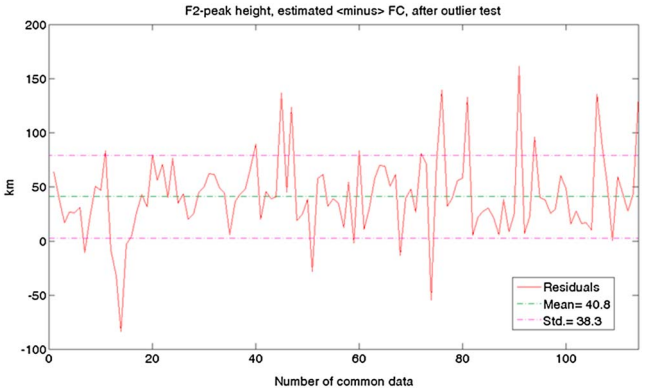

Figure 10. F_2 peak height deviations of estimated minus F/C, for day 182, 2010 [0,2] UT.

z has a normal probability density function with $\mu = 0$ and standard deviation s

$$z \sim \mathcal{N}(0, s) \ . \tag{36}$$

The statistical test is performed and the null hypothesis of "$\mu = 0$" is accepted with a confidence interval of $1 - \alpha = 0.90$, for both N_m and h_m values. This means that the difference between estimated N_mF_2 and h_mF_2 and the corresponding values derived from F/C is statistically insignificant with a confidence level of 90%.

8. Conclusions and Outlook

In this study, we investigated on global 3-D modeling of electron density using simulated GNSS measurements. To model the electron density, the upper atmosphere was assumed to be a stratified layer with three major subdivisions, i.e., the bottomside ionosphere, ranging from 50 to 200 km, the topside ionosphere from 200 to 1000 km, and the plasmasphere from 1000 to 2000 km. As a first step, the plasmaspheric contribution was assumed to be known; therefore, we concentrated only on the ionospheric part. According to the Chapman profile function, electron density at any point is given by the F2 maximum electron density and its corresponding height. So the aim was to model N_mF_2 and h_mF_2 in globe. For this goal, two sets of spherical harmonic expansions were applied to the GNSS ionospheric observable, which relates the GNSS input data to the F_2 peak parameters. To perform the estimation, GNSS input data were simulated in such a way that the true positions of the satellites were detected and used, but the STEC values were obtained through a simulation procedure, using the IGS VTEC maps. After simulating the input data, the a priori values required for the estimation procedure were calculated using the IRI-2012 model and also by applying the ray tracing technique. In the course of the estimation, appropriate constraints were applied to avoid unrealistic large residuals. The procedure was performed for a sample day, 1 July 2010, and the models were depicted as global grid-wise maps. To evaluate the results, first the RMS maps of estimated N_mF_2 and h_mF_2 were established by applying error propagation law to the covariance matrix of the estimated spherical harmonic coefficients. In the second step, the estimated N_mF_2 and h_mF_2 were compared with the F_2 peak parameters derived from F/C data.

The comparisons prove that the developed 3-D models of electron density peak parameters have a great potential to reconstruct the electron density profiles over the globe. These profiles provide information about the ionosphere at different altitudes. This is in particular useful when, e.g., satellite to satellite observation is being performed. Besides the geodetic applications, this 3-D modeling approach can include geophysical parameters with high resolution, which is essential in all studies of the upper atmosphere, space weather, and for the solar-terrestrial environment.

Our next steps will be (a) improvement of the accuracy and reliability of the results by studying the approximating assumptions and their influence on the resulting output; (b) applying this procedure to longer time spans, i.e., at least several days and for different solar conditions. We also plan to implement real GNSS data instead of simulated data and to estimate the plasmaspheric key parameters, i.e., the plasma scale height H_P and the plasmasphere basis density N_P. Finally, information from other space geodetic techniques will be integrated into our modeling approach. This can improve the accuracy of the developed maps by closing the gap within GNSS input data.

Acknowledgments

The authors wish to express their gratitude to Dudy D. Wijaya (currently at Geodesy Research Group, Bandung Institute of Technology, Indonesia) for providing the MATLAB codes for applying ray tracing technique. Many thanks to the International GNSS Service (IGS) (http://igscb.jpl.nasa.gov/) for the free supply of ionospheric data, the International Reference Ionosphere (IRI) for providing free Fortran source code for ionospheric parameter computation (ftp://nssdcftp.gsfc.nasa.gov/models/), and Lung-Chi Tsai from the Ionolab, Taiwan National University (http://isarncu.ncu.edu.tw/en-us/index.html) for providing F_2 peak parameters from the F/C radio occultation data. This study was accomplished within the project MDION (P22203-N22) funded by the Austrian Science Fund (FWF).

References

Alizadeh, M. M. (2013), Multi-dimensional modeling of the ionospheric parameters, using space geodetic techniques, PhD thesis, Geowissenchaftliche Mitteilungen Heft Nr. 93, Vienna Univ. of Technology, ISSN 1811-8380.

Alizadeh, M. M., H. Schuh, S. Todorova, and M. Schmidt (2011), Global ionosphere maps of VTEC from GNSS, satellite altimetry, and Formosat-3/cosmic data, *J. Geod.*, *85*(12), 975–987.

Bilitza, D., and B. W. Reinisch (2007), International reference ionosphere 2007: Improvements and new parameters, *Adv. Space Res.*, *42*, 599–609.

Bilitza, D., L. A. McKinnell, B. Reinisch, and T. Fuller-Rowell (2011), The international reference ionosphere today and in the future, *J. Geod.*, *85*, 909–920.

Born, M., and E. Wolf (1999), *Principles of Optics*, 7th ed., Cambridge Univ. Press, New York.

Brunner, F. K., and M. Gu (1991), An improved model for the dual frequency ionospheric correction of GPS observations, *Manuscripta Geod.*, *16*, 205–214.

Cappellari, J. O., C. E. Velez, and A. J. Fuchs (1976), Mathematical theory of the Goddard trajectory determination system, *Tech. Rep. NASA-TM-X-71106, X-582-76-77*, NASA Goddard Space Flight Center, Greenbelt, Md.

Chiu, Y. T. (1975), An improved phenomenological model of ionospheric density, *J. Atmos. Terr. Phys.*, *37*, 1563–1570.

Datta-Barua, S., T. Walter, J. Blanch, and P. Enge (2006), Bounding higher order ionosphere errors for the dual frequency GPS user, in *Proceeding of ION GNSS*, pp. 1377–1392, Inst. of Nav., Forth Worth, Tex.

Davies, K. (1990), *Ionospheric Radio*, Peter Peregrinus Ltd., London, U. K.

Ezquer, R. G., M. M. de González, and T. Heredia (1996), Electron density profile modeling, *Ann. Di Geof.*, *39*(3), 539–542.

Feltens, J. (1998), Chapman profile approach for 3-D global tec representation, in *Proceedings of the IGS VTEC Maps Analysis Centers Workshop*, pp. 285–297, ESOC, Darmstadt, Germany, 9-11 February, IGS Presentation.

Feltens, J. (2003), The International GPS Service (IGS) ionosphere working group, *Adv. Space Res.*, *31*(3), 205–214.

Feltens, J., et al. (2010), GNSS contribution to next generation global ionospheric monitoring, *Tech. Rep.*, ESA/ESOC Final Report, DOPS-SYS-RP-5001-OPS-GN.

Fremouw, E., J. A. Secan, and B. M. Howe (1992), Application of stochastic inverse theory to ionospheric tomography, *Radio Sci.*, *27*(5), 721–732.

Hernández-Pajares, M., J. M. Juan, J. Sanz, R. Orús-Perez, A. García-Rigo, J. Feltens, J. Komjathy, S. C. Schaer, and A. Krankowski (2009), The IGS VTEC maps: A reliable source of ionospheric information since 1998, *J. Geod.*, *83*(3–4), 263–275.

Hochegger, G., B. Nava, S. M. Radicella, and R. Leitinger (2000), A family of ionosphericmodels for different uses, *Phys. Chem. Earth Part C: Sol. Terr. Planet Sci.*, *25*(4), 307–310.

Howe, B. M., K. Runciman, and J. A. Secan (1998), Tomography of the ionosphere: Four-dimensional simulations, *Radio Sci.*, *33*(1), 109–128.
Huang, X., B. W. Reinisch, P. Song, J. L. Green, and D. L. Gallagher (2004), Developing an empirical density model of the plasmasphere using IMAGE/RPI observations, *Adv. Space Res.*, *33*, 829–832.
Jakowski, N., I. S. Kutiev, S. Heise, and A. Wehrenpfennig (2002), A topside ionosphere-plasmasphere model for operational applications, in *Proceeding of URSI XXVII General Assembly*, pp. 2174–2177, Maastricht, Netherlands.
Nafisi, V., M. Madzak, J. Böhm, A. A. Ardalan, and H. Schuh (2012), Ray-traced tropospheric delays in VLBI analysis, *Radio Sci.*, *47*, RS2020, doi:10.1029/2011RS004918.
Newby, S. P. (1992), An assessment of empirical models for the prediction of the transionospheric propagation delay of radio signals, *Tech. Rep. 160*, Dep. of Surv. and Eng., Univ. of New Brunswick, Canada.
Radicella, S. M., and R. Leitinger (2001), The evolution of the DGR approach to model electron density profiles, *Adv. Space Res.*, *27*(1), 35–40.
Ratcliffe, J. A. (1972), *An Introduction Into the Ionosphere and Magnetosphere*, chap. 2.3-2.4, Cambridge Univ. Press, London.
Rawer, K. (1988), Synthesis of ionospheric electron density profiles with Epstein functions, *Adv. Space Res.*, *8*(4), 191–198.
Rishbeth, H., and O. K. Garriott (1969), *Introduction to Ionospheric Physics*, Academic Press, New York.
Schaer, S. (1999), Mapping and predicting the Earth's ionosphere using the Global Positioning System, PhD thesis, Bern Univ., Switzerland.
Schaer, S., W. Gunter, and J. Feltens (1998), Ionex: The ionosphere map exchange format version 1, in *Proceeding of the IGS AC Workshop*, edited by J. M. Dow, J. Kouba, and T. Springer, pp. 233–247, Eur. Space Cent. of the Eur. Space Agency, Darmstadt, Germany.
Schunk, R. W., L. Scherliess, J. J. Sojka, and D. Thompson (2004), Global Assimilation of Ionospheric Measurements (GAIM), *Radio Sci.*, *39*, RS1S02, doi:10.1029/2002RS002794.
Teunissen, P. J. G., and A. Kleusberg (1998), *GPS for Geodesy*, Springer, Berlin.
Todorova, S. (2008), Combination of space geodetic techniques for global mapping of the ionosphere, PhD thesis, Austria.
Tsai, L. C. (2012), *Ionospheric sounding lab*. [Available at http://isarncu.ncu.edu.tw/en-us/index.html.]
Tsai, L. C., K.-C. Cheng, and C. H. Liu (2011), GPS radio occultation measurements on ionospheric electron density from low Earth orbit, *J. Geod.*, *85*(12), 941–948.
Wijaya, D. D. (2010), Atmospheric correction formulae for space geodetic techniques, PhD thesis, Technische Univ. Graz, Graz, Austria.